Phase-based Regional Oxygen Metabolism in Magnetic Resonance Imaging at High Field

by

Audrey Peiwen Fan

B.S. Electrical Engineering, B.S. Biological Sciences

Stanford University, 2008

Submitted to the Department of Electrical Engineering and Computer Science in Partial Fulfillment of the Requirements for the Degree of

Master of Science in Electrical Engineering and Computer Science

at the

MASSACHUSETTS INSTITUTE OF TECHNOLOGY

JUNE 2010

Signature of Author _____

Department of Electrical Engineering and Computer Science
May 21, 2010

Certified by _____

Elfar Adalsteinsson
Associate Professor of Electrical Engineering and Computer Science
Associate Professor of Harvard-MIT Health Sciences & Technology
Thesis Supervisor

Accepted by _____

Terry P. Orlando
Professor of Electrical Engineering and Computer Science
Chairman, EECS committee of Graduate Students

Phase-based Regional Oxygen Metabolism in Magnetic Resonance Imaging at High Field

by

Audrey Peiwen Fan

Submitted to the Department of Electrical Engineering and Computer Science

May 21, 2010

In Partial Fulfillments of the Requirements for the Degree of Master of Science in Electrical Engineering and Computer Science

ABSTRACT

Venous oxygen saturation (Y_v) in cerebral veins and the cerebral metabolic rate of oxygen ($CMRO_2$) are important indicators for brain function and disease. Phase-susceptibility measurements in magnetic resonance imaging (MRI) have been used to quantify Y_v in candidate cerebral veins. However, currently there is no method to quantify regional $CMRO_2$ using MRI. Here we propose a novel technique to quantify $CMRO_2$ from independent MRI estimates of Y_v and cerebral blood flow (CBF). Our approach used standard gradient-echo (GRE) and arterial spin labeling (ASL) to make these measurements. Results for *in vivo* Y_v and $CMRO_2$ estimates on human subjects are presented from application of our technique at 3 Tesla (3T). We also extended our method to high-field human imaging at 7 Tesla (7T), which allows us to take advantage of improved signal-to-noise ratio (SNR) for the same scan duration to achieve higher-resolution analysis of vessels of interest. While the higher field strength poses additional challenges, such as increased main field and excitation field inhomogeneities as well as more severe susceptibility artifacts, initial results suggest that substantial benefits can be realized with phase-based regional oxygen metabolism in MRI at high field.

Thesis Supervisor: Elfar Adalsteinsson

Title: Associate Professor of Electrical Engineering and Computer Science
Associate Professor of Harvard-MIT Health Sciences & Technology

Acknowledgements

I am very grateful for all the people who have been a big part of my life these past two years. First and foremost I want to thank my advisor Professor Elfar Adalsteinsson, whose patience and encouragement have allowed me to grow so much. It is rare to find an advisor as loyal and supportive as Elfar, and for that I am extremely lucky. I also want to thank my secondary advisor Professor Bruce Rosen for his mentorship and insightful perspective. His constant enthusiasm for my project is truly refreshing.

My officemate Div has been a great role model for me, and my first years in graduate school would have been completely different without him. I thank Thomas Benner for sticking it out at Bay 5 with me and for teaching me to become a more independent researcher. I also want to thank Trina, Borjan, Joonsung, Lohith, and Berkin for being the best labmates I could ever ask for. Some of my best memories at MIT are of hanging out with them.

I am eternally thankful for my mom and dad, who have given me endless love and provided me with so many opportunities to soar. My sisters Kathy, Denise, and Lily are amazing people, and each holds a special place in my heart that gives me inspiration and keeps me sane. Finally, I want to thank Harvey for always being there for me. You are a blessing in my life, and I am so happy that I get to share my time in Boston with you.

Our work was done in collaboration with the Athinoula A. Martinos Center for Biomedical Imaging. This work is supported by the Advanced Multimodal Neuroimaging Training Program (T90DA022759) and the *Siemens-MIT* Alliance.

Contents

List of Figures and Tables

Chapter 1

Introduction

While magnetic resonance imaging (MRI) does not offer a direct contrast mechanism for tissue oxygenation or oxygen consumption, the complicated physiology of blood flow and oxygenation in the brain does modulate the MRI signal. Neural activity creates local changes in cerebral hemodynamics, which in turn can be detected using functional magnetic resonance imaging (fMRI) techniques through the blood-oxygen-level-dependent (BOLD) response [1, 2]. The BOLD effect is a complex function of cerebral hemodynamics, including cerebral blood flow (CBF), cerebral blood volume (CBV), and oxygen consumption [3, 4], and relative changes in this hemodynamic response are used as a surrogate to detect neuronal activity.

Despite recent advances in high-resolution imaging, BOLD fMRI offers limited temporal and spatial resolution of brain function. Ideally, measured hemodynamic changes reflect physiological alterations in the capillary bed where oxygen exchange between the cerebral vessels and tissue occurs during neural activation. However, the specificity of the technique is difficult to assess because measurements may be contaminated by larger vessels with higher

metabolic activity [1, 5]. This limits localization of activation regions and estimation of their extent, especially as exact models relating the BOLD signal to underlying physiological changes are difficult to establish.

Unlike the BOLD mechanism for contrast, venous oxygen saturation (Y_v) and the cerebral metabolic rate of oxygen ($CMRO_2$) are quantitative physiological parameters. Y_v is a measure of the percentage oxygen saturation remaining in cerebral veins, and $CMRO_2$ (μmol/g/min) is a metabolic parameter that quantifies the rate of oxygen expenditure in brain tissue. As fundamental physiological parameters, both are important indicators of tissue viability. Absolute measurements of $CMRO_2$ and Y_v are thus expected to be intrinsically linked to underlying physiological processes [6, 7], and regional estimates of these parameters would provide new information about neural function and modulation in disease states of the brain.

Currently, there is no direct method to measure regional Y_v and $CMRO_2$ with MRI in the human brain. Accepted values for Y_v and $CMRO_2$ in the literature are reported by positron emission tomography (PET) studies [8] and have identified these parameters as critical markers in disease states such as stroke and tumor [9, 10]. However, PET imaging is a comparatively low spatial-resolution technique and involves injection of a radioactive label, which requires equipment that is not widely available. MRI-based methods have been proposed to measure oxygenation in the brain, including the combination of fMRI BOLD and CBF measurements for calibrated estimates of $CMRO_2$ changes [11]. These calibrated fMRI techniques, however, only measure relative changes in metabolism and depend on a physiological challenge such as hypercapnia, or inhalation of air mixed with CO_2. A recent alternate approach based on T_2 relaxation in MRI, T2-relaxation-under-spin-tagging (TRUST), allows quantification of absolute Y_v and $CMRO_2$, but only offers global measurements from the whole brain [12].

Our goal is provide high-resolution, quantitative measurements of local $CMRO_2$ and Y_v currently unavailable in MRI. Here, we present a novel approach to quantify localized $CMRO_2$ from independent measures of Y_v and CBF. MR phase-susceptibility techniques have been used to measure global and regional venous oxygenation in resting and activated states of the brain at 3 Tesla (3T) [13, 14]. Our measurements of venous oxygen saturation are based on innate susceptibility differences between cerebral blood vessels and the surrounding brain parenchyma. The measured susceptibility differences are related to oxygen saturation because the intravascular concentration of deoxyhemoglobin (dHb), a paramagnetic species, changes with vessel oxygenation. We acquire gradient-echo phase maps using MRI, from which susceptibility changes and the corresponding Y_v can be quantified for candidate veins amenable to our assumptions about vessel geometry.

To quantify $CMRO_2$, we acquire an additional CBF measurement using arterial spin labeling (ASL) with MRI. ASL includes a noninvasive tagging scheme that magnetically labels arterial blood flowing into an imaging slice and can provide a quantitative perfusion map for the slice [15]. We use ASL to measure local tissue CBF representative for our cerebral vessels of interest. $CMRO_2$ is then quantified on a regional basis through a known relationship with CBF and Y_v, the Fick principle of arterio-venous difference [5, 16]. Here we present results for Y_v and $CMRO_2$ using this method in human subjects at 3T.

The power of our technique is that it uses standard sequences readily available on clinical scanners and can be generalized for improved local measurements throughout the brain. We have extended our technique to high field at 7 Tesla (7T), which offers improved signal-to-noise ratio (SNR) that allows for higher-resolution imaging. Challenges of high-field imaging include more severe field inhomogeneity, phase wrapping, and background susceptibility gradients. We

address some of these issues to take advantage of improved resolution at high field and present preliminary *in vivo* measurements of Y_v and $CMRO_2$ at 7T. In addition, recent developments in quantitative susceptibility mapping [17–22] suggest that our method can be generalized to a larger set of veins without the constraints on vessel geometry or orientation present in the current technique. We will discuss these promising improvements to our method as well as potential applications of our high-resolution measures of local Y_v and $CMRO_2$ in future work.

The work presented in this thesis was accepted as an oral presentation at the 18^{th} annual meeting of the International Society for Magnetic Resonance in Medicine (ISMRM), held recently in Stockholm, Sweden.

Chapter 2

Background

2.1 Phase-susceptibility measurements of vessel oxygenation

Magnetic susceptibility (χ) is a quantitative measure of the magnetization of a material in response to an applied magnetic field. For materials whose magnetization M is linearly related to the applied magnetic field H, susceptibility is a dimensionless quantity defined as $\chi = M / H$, where M and H both have units of Amperes/m [23]. Materials can be classified according to susceptibility as paramagnetic ($\chi>0$), diamagnetic ($\chi<0$), and ferromagnetic ($\chi>>0$). Paramagnetic materials tend to increase the surrounding applied field and diamagnetic materials tend to decrease this field. Most materials important in MRI are weakly magnetic with $|\chi| < 0$, and values for common biological materials in MRI are presented in *Fig 1* [23].

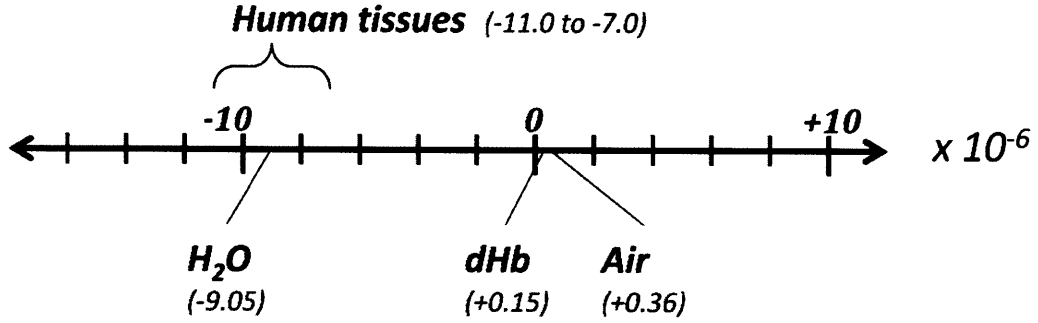

Figure 1. Absolute susceptibility of common biological materials in MRI. Deoxyhemoglobin is denoted dHb.

The susceptibility difference ($\Delta\chi$) between venous blood vessels and the surrounding brain tissue is related to venous oxygenation (Y_v), our parameter of interest. This section describes how our method uses phase measurements to quantify this susceptibility shift and thus the underlying vessel oxygenation.

2.1.1 Susceptibility shift between a vein and background tissue is related to venous oxygen saturation

We are motivated to measure the susceptibility shift between a vein and the surrounding tissue because it provides endogenous oxygenation-dependent contrast *in vivo*. Hemoglobin in red blood cells is the primary carrier of oxygen in the body, and its reduced form, deoxyhemoglobin (dHb), is found in venous blood. Decreased oxygenation corresponds to increased concentration of dHb, which is known to be paramagnetic. This reflected in the increased susceptibility of venous blood with respect to the surrounding brain parenchyma.

From the measured susceptibility shift $\Delta\chi_{vein\text{-}tissue}$, we quantified oxygen saturation Y_v for each vessel using *Equation 1* [13]. Here we assumed $\Delta\chi_{do} = 0.18$ ppm (cgs) as the susceptibility difference between fully deoxygenated and fully oxygenated blood [24], where implicitly the tissue has the same susceptibility as fully oxygenated blood. We also assumed literature values for hematocrit, or the percent fraction of blood volume that consists of red blood cells, where *Hct* = 0.42 for males and *Hct* = 0.38 for females [25].

$$\Delta\chi_{vein-tissue} = \Delta\chi_{do} \cdot Hct \cdot (1 - Y_v) \qquad (Eq.\ 1)$$

2.1.2 Relationship between local susceptibility shift and magnetic field shift

MRI is sensitive to local perturbations in the main magnetic field (B_0), including those that arise from susceptibility effects. We are interested in the field difference between the inside of the vein of interest and the surrounding tissue, $\Delta B_{vein\text{-}tissue}$. Although this local field shift is related to the underlying susceptibility difference $\Delta\chi_{vein\text{-}tissue}$ we are trying to measure, it is also highly dependent on vessel geometry and orientation. For this reason, the inversion from a field map to susceptibility map is not straightforward.

Recent developments have allowed for rapid simulation of the expected field map from the underlying susceptibility distribution [26, 27]. This is described in *Equation 2*, where ΔB is expressed in the image domain with spatial coordinates and *FT* refers to a three-dimensional Fourier Transform. Here, the magnitude of a k-space vector, $k^2 = k_x^2 + k_y^2 + k_z^2$, is calculated for

each point in the k-space (Fourier) domain, and k_z refers to the component of the k-space vector parallel to the main magnetic field [19].

$$\Delta B(x,y,z) = B_0 \cdot FT^{-1}\left[\left(\frac{1}{3} - \frac{k_z^2}{k^2}\right) \cdot FT\{\chi(x,y,z)\}\right] \qquad (Eq.\ 2)$$

Although *Equation 2* allows for fast forward calculation of the field map, the inversion problem critical for our technique is difficult in general. The inversion is ill-posed for a conical region in k-space of angle 54.1^0, where the factor $\frac{1}{3} - \frac{k_z^2}{k^2} = 0$, because the k-space data is effectively lost in that region.

In our method, we focused on candidate veins for which the inversion from measured field shift to susceptibility shift is straightforward. Weisskoff and Kiihne first developed an MRI method to quantify absolute susceptibility by imaging phase of paramagnetic agents in cylindrical tubes, including red blood cells at various oxygenations [24]. Haacke applied this technique to cerebral vessels *in vivo* [13], and we adopted similar assumptions about vessel geometry and orientation in our method. Here we used axial imaging slices, which are orthogonal to the direction of the main magnetic field, B_0. We restricted our analysis to through-plane vessels parallel to B_0, with a diameter much smaller than the length of the vessel segment along the main field (*Fig 1*).

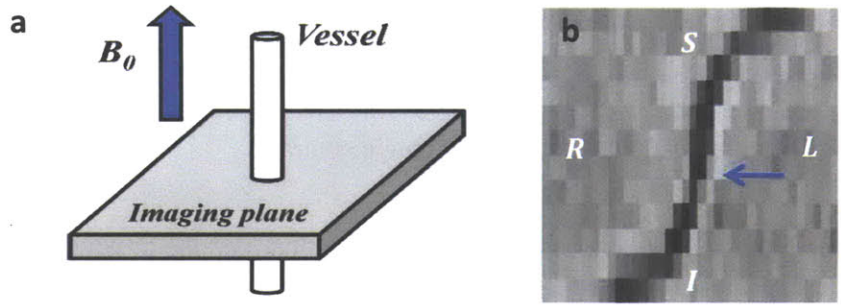

Figure 2. (**a**) Schematic of geometry and orientation of candidate through-plane vessels in axial imaging plane. (**b**) Example of coronal view of candidate vessel *in vivo*. The blue arrow indicates slice from which phase measurements are made. *S* = superior, *R* = subject right, *L* = subject left, *I* = inferior.

For the purpose of estimating field changes due to susceptibility variation between the inside and outside of the vein, such vessels are approximated as infinite cylinders, for which there is a simple analytical relationship between ΔB and Δχ. In this case, the ill-conditioned relationship in *Equation 2* reduces to a simple proportionality between ΔB and Δχ (*Equation 3*), which dramatically simplifies the estimation of Δχ. This approximation holds well even if the vessel is slightly tilted with respect to the main magnetic field, with less than 5% error in the estimated oxygen saturation from simulation for vessel tilt of less than 10^0 [14].

$$\Delta B_{vein-tissue} = \frac{1}{3} 4\pi \cdot \Delta\chi_{vein-tissue} \cdot B_0 \qquad (Eq.\ 3)$$

2.1.3 Gradient-echo phase images reveal local field shifts

The gradient-echo (GRE) sequence in MRI uses a pair of bipolar gradients to create a signal echo for imaging [28]. This image encoding method is summarized by a pulse sequence diagram, which displays the relative timing of the radiofrequency (RF) excitation pulse, gradient

pulses, and the data sampling period or ADC. For the GRE sequence, a representative pulse sequence diagram is shown in *Fig 2*, where acquisition parameters such as the flip angle (α^0), echo time (TE), and the repetition time (TR) determine the image contrast.

GRE imaging can be implemented as a relatively fast acquisition, i.e. one in which TR is short, such that acquiring several hundred TR periods for an image with appropriate resolution takes a few minutes. For our studies, we applied a standard implementation of GRE called Fast Low-Angle Shot (FLASH) [29]. We also used first-order flow compensation, or gradient moment nulling, in three directions to minimize flow-related artifacts from the blood in our phase measurements [28].

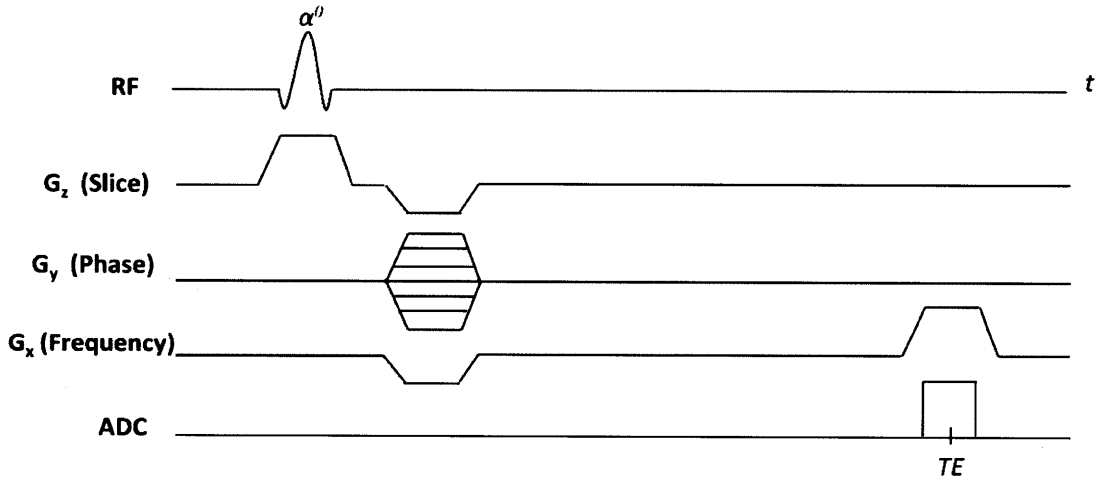

Figure 3. Pulse sequence diagram for gradient-echo acquisition. The flip angle is denoted α^0 and ADC represents the signal readout at time TE.

With the assumptions previously described, local field shifts manifested in gradient-echo phase images can be measured as a proxy for susceptibility measurements to quantify Y_v. The resulting magnitude images are sensitive to T_2* relaxation effects, i.e. the decay of the MR signal during TE, including susceptibility-induced field perturbations between the vein and tissue.

Since dHb in cerebral veins is paramagnetic, we expect the field inside the vessel to be increased with respect to the brain parenchyma, so that cerebral veins have bright contrast in phase images. The same vessels appear dark in GRE magnitude images because signal loss occurs due to dephasing from $\Delta B_{vein\text{-}tissue}$.

We acquired gradient echo images at multiple echo times (TE), and measure phase differences between the vessel and background tissue to determine the local field shift. The phase evolves linearly with TE as described by the Larmor relationship in *Equation 4*, where $\gamma = 2.67 \cdot 10^8$ rad/(s · T) is the gyromagnetic ratio for a ^{1}H proton.

$$\Delta\varphi_{vein-tissue} = \gamma \cdot TE \cdot \Delta B_{vein-tissue} \qquad (Eq.4)$$

2.2 Quantification of cerebral blood flow (CBF) with arterial spin labeling (ASL)

To quantify regional neural metabolism, our technique uses arterial spin labeling (ASL) for local measures of perfusion in the brain [30, 31]. In ASL, a tag image and control image are generated. For the tag image, a 180^0 inversion pulse is used to invert spins in arterial blood before it reaches the imaging slice. The tag image is generated after a user-specified inflow time (TI) during which labeled spins are carried by arterial blood into the imaging slice at a rate proportional to local perfusion. A control image is then acquired with the same sequence

parameters but without the magnetic tagging of the blood. When the tag image is subtracted from the control image, static spins cancel out, and each voxel in the difference image is proportional to local cerebral blood flow (CBF), the rate of delivery of arterial blood [15].

2.2.1 PICORE-Q2TIPS acquisition avoids venous signal contamination and transit delay effects

In our method, we used a pulsed ASL scheme with an echo-planar imaging (EPI) acquisition. Our acquisition applied PICORE (proximal inversion with control for off-resonance effects) tagging, which uses a spatially-selective pulse to invert spins flowing through a thick band below the slice of interest to be imaged (*Figure 3a*) [32]. Because PICORE tagging only uses one inversion band below the imaging slice, it is sensitive only to arterial blood flow. This avoids potential venous blood contamination that can be a problem in other ASL tagging schemes such as FAIR (flow sensitive alternating inversion recovery) that includes non-selective inversion both below and above the imaging slice [15].

In pulsed ASL, there is a transit delay (δt) for flowing spins that arises from the necessary gap between the inversion band and the imaging slice. This delay can create errors in quantitative CBF measurements, especially in disease states of the brain in which the vascular path is impaired. QUIPSS II (quantitative imaging of perfusion using a single subtraction) is a refinement to the ASL sequence that mitigates transit delay effects. After the original inversion pulse to label arterial blood, QUIPSS II applies a saturation pulse in the same location as the inversion band at a time TI_1 (*Fig 4b*) [33]. This ensures that the final perfusion only comes

from a blood tagged during the time period up to the specified TI_1, i.e. it effectively defines a bolus of labeled spins with width TI_1. If the image is then acquired at a time TI_2 after all the labeled blood has enough time to travel to the imaging slice, we can avoid transit delay errors in our quantitative perfusion map. That is, TI_2 should be chosen such that $TI_2 \geq TI_1 + \delta t$.

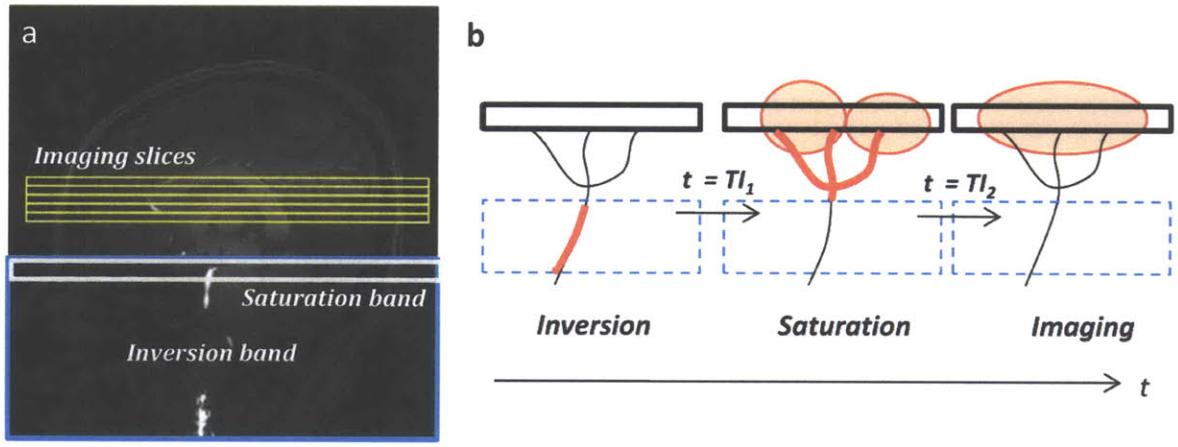

Figure 4. (**a**) Axial positioning of imaging slices and inversion and saturation bands for PICORE-Q2TIPS ASL acquisition. (**b**) QUIPSS II schematic illustrating application of saturation in the same location of inversion band at time $t = TI_1$. Imaging occurs after all tagged blood has reached the capillary bed in the imaging slice at time $t = TI_2$.

Q2TIPS (QUIPSS II with thin-slice TI_1 periodic saturation) replaces the single saturation band in QUIPSS II with a train of saturation pulses at the distal end of the inversion band at a time TI_1 [34]. These saturation pulses have a thinner sinc slice profile to create sharper edges than the thicker profile of the original saturation band, and offer improved B_1 field homogeneity. These refinements have been shown to improve the accuracy of quantitative CBF maps.

2.2.2 Calibration of ASL images for quantitative CBF

The PICORE-Q2TIPS acquisition provides a control-tag subtraction series that can be averaged for a relative perfusion map. To calibrate the CBF measurement, we acquire an additional scan with matched TR and TE to estimate the fully relaxed longitudinal magnetization of arterial blood (M_{0B}) on a voxel-by-voxel basis from the local tissue equilibrium magnetization. The flow was then quantified from the averaged difference signal (ΔM) using *Equation 5*, where CBF is measured in units of ml/100g/min [15].

$$\Delta M = 2 M_{0B} \cdot CBF \cdot TI_1 \cdot e^{-TI_2 / T_{1b}} \qquad (Eq.5)$$

Here, TI_1 and TI_2 are parameters set by the user and T_{1b} is the T_1 relaxation constant of blood. The factor of 2 arises because we subtract inverted spins in the tag image from the control image, and the exponential term represents T_1 decay that occurs until imaging at time TI_2. We have assumed T_{1b} = 1684 ms at 3 Tesla [15], and T_{1b} = 2000 ms at 7 Tesla [35]. Note that ΔM is proportional to the bolus width TI_1, and to our measurement of interest, CBF.

2.3 The Fick principle of arterio-venous difference relates $CMRO_2$ to Y_v and CBF

The Fick principle has been used to relate flow, the arterio-venous oxygenation gradient, and oxygen consumption [5, 12]. We use the Fick principle to quantify $CMRO_2$ in

μmol/100g/min from our previously described measurements. As described in *Equation 6*, $CMRO_2$ is proportional to the oxygen extraction fraction (OEF) and local perfusion around a vessel of interest. OEF is calculated from Y_v as in *Equation 7*, where we have assumed that arterial blood is fully saturated ($Y_a = 100\%$). The total concentration of hemoglobin, [*Hb*], can be calculated from the assumed hematocrit (*Hct*) values using *Equation 8*, where $0.016125g$ is the micromolar mass of one *Hb* unit.

$$\boldsymbol{CMRO_2 = OEF \cdot [Hb] \cdot CBF \cdot Y_a} \qquad \textbf{(Eq.6)}$$

$$\boldsymbol{OEF = \frac{Y_a - Y_v}{Y_a}} \qquad \textbf{(Eq.7)}$$

$$\boldsymbol{[Hb] = \frac{Hct}{3.0 \cdot 0.016125}} \qquad \textbf{(Eq.8)}$$

Chapter 3

Methods

3.1 Phase-susceptibility measurements using 2D gradient-echo at 3T

We acquired 10 axial slices with both magnitude and phase contrast using the 2D, flow-compensated FLASH sequence detailed in *Table 1*. Here the listed acquisition time is for each echo as they were acquired in separate scans to maintain flow compensations at all echo times.

Table 1. **GRE sequence parameters at 3T**

Sequence	*fl2d1r*	**Acquisition time (min)**	5:53
TR (ms)	270	**Field of view (mm)**	217 x 224
TE (ms)	10, 15, 20	**Resolution (mm)**	0.5 x 0.5 x 2.0
Flip Angle (deg)	25	**Bandwidth per pixel (Hz/pix)**	151

3.1.1 Selection of echo times (TE) for phase-susceptibility measurements

To optimize the range of GRE echo times, we simulated the expected phase difference between the vessel and tissue for physiological oxygenation levels. This involved a tradeoff between larger values for the accrued phase at longer TE's versus less T_2* signal decay and less phase wrapping at shorter TE's. As a compromise, we used echo times of $TE = 5, 10, 15ms$ for our 3T acquisition to avoid phase wrapping between the vessel and background tissue (*Fig 4a*), while maintaining a maximum expected phase difference of between 2 and 3 radians for the physiological range of Y_v (50 – 75%) [14].

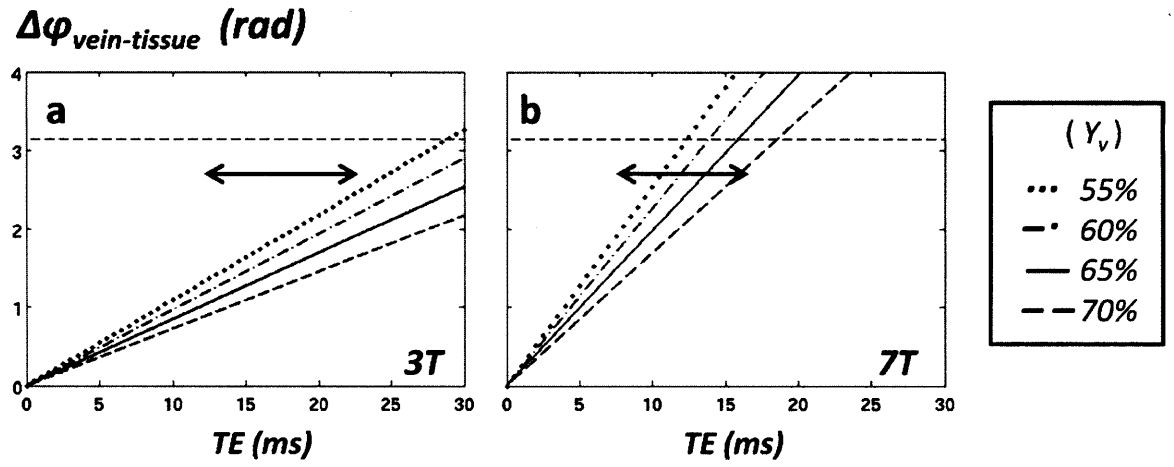

Figure 5. Simulated phase difference between vein and tissue for various oxygenation levels at (**a**) 3T and (**b**) 7T. Black arrows indicate the range of TE's used in our GRE acquisition for each field strength, and the black dotted line is at a phase difference of pi.

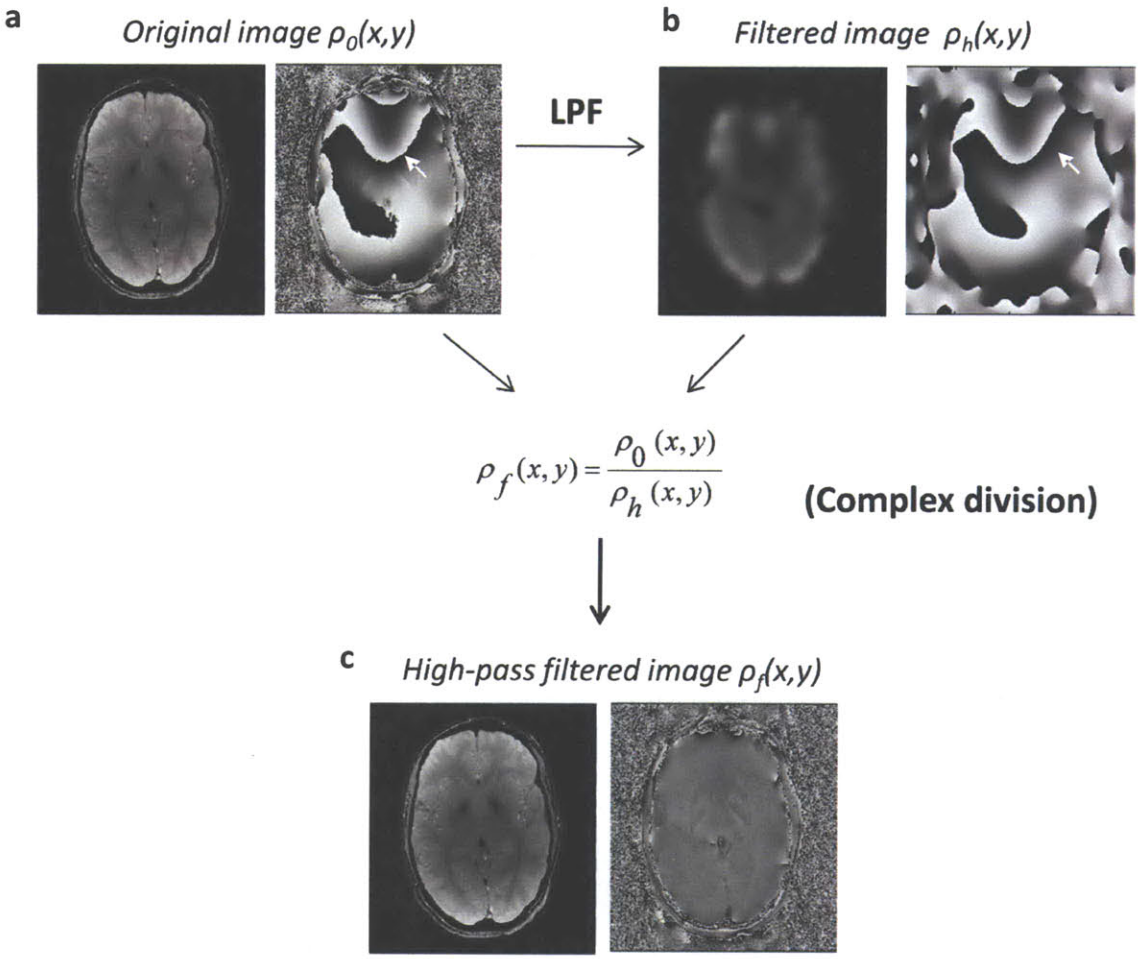

Figure 6. Schematic for high-pass filtering of phase images from GRE acquisition. (**a**) Magnitude and phase of original GRE image. White arrow illustrates an example of phase-wrapping. (**b**) Low-pass filtered magnitude and phase. Notice that the phase-wrapping artifact is still present because it is not a physical attribute of the complex image. (**c**) Final high-pass filtered phase image after complex division as proposed in [32].

3.1.2 High-pass filtering of phase images at 3T to remove background inhomogeneities

Background field inhomogeneities cause low-frequency spatial variations in the gradient echo phase image. These background phase effects must be removed before quantitative measurements can be made. At 3T, the gradient-echo phase images are effectively high-pass

filtered by dividing the original complex signal by a low-pass filtered version of the image (*Fig 5*) [36]. The low-pass filter is implemented with a 32 x 32 pixel 2D Hanning filter in k-space, as proposed by Wang et al [36]. This technique removes phase-wraps in the phase image, and the resulting background tissue has more homogenous phase with mean value of approximately zero.

3.2 Arterial spin labeling acquisition at 3T

We acquired cerebral blood flow maps using the PICORE-Q2TIPS acquisition [28, 30] described in *Table 2*. For each scan, 90 control-tag pairs were averaged to generate the perfusion maps. Note that the ASL sequence has lower in-plane resolution and twice the slice thickness of the FLASH scans. We matched the coverage of the ASL scans to that of the GRE acquisition and selected the appropriate slice to measure local perfusion in our analysis.

Table 2. **PICORE-Q2TIPS ASL sequence parameters at 3T**

Sequence	*epfid2d1*	**Acquisition time (min)**	9:03
TR (ms)	2300	**Field of view (mm)**	220 x 220
TI_1 /TI_2 (ms)	700 / 1800	**Resolution (mm)**	2.0 x 2.0 x 4.0
TE (ms)	25	**Bandwidth per pixel (Hz/pix)**	1570

3.3 Quantification of Y_v and $CMRO_2$

Candidate gray matter veins for our measurements with were identified manually through several gradient echo slices (*Fig 5a*). The appropriate vessel geometry was confirmed using a sagittal or coronal view of the selected vein (*Fig 1b*). To measure $\Delta\varphi_{vein\text{-}tissue}$ for each TE, we used the maximum phase value inside the vein for φ_{vein} to avoid partial-volume effects (*Fig 5b*). Partial-volume effects occur when signal for several tissue types are averaged within a voxel. Y_v was calculated only for vessels that demonstrated a robust fit of $\Delta\varphi_{vein\text{-}tissue}$ across TE's, with $R^2 > 0.95$ (*Fig 5d*).

Local perfusion for each vein analyzed was analyzed by averaging CBF values from a 6.0 x 6.0*mm* region in the appropriately matched CBF slice (*Fig 5b*). Regional $CMRO_2$ was then calculated for each candidate vessel using the measured Y_v and local CBF.

3.4 Extension to high field imaging at 7T

Imaging at 7T offers significant improvements to SNR that allow for higher resolution acquisitions. However, main field and radiofrequency (RF) field inhomogeneities and background susceptibility gradients pose more difficult problems at high field. Here we present our methods at 7T, which include different acquisition parameters and more aggressive filtering to deal with phase-wrapping and increased field inhomogeneities.

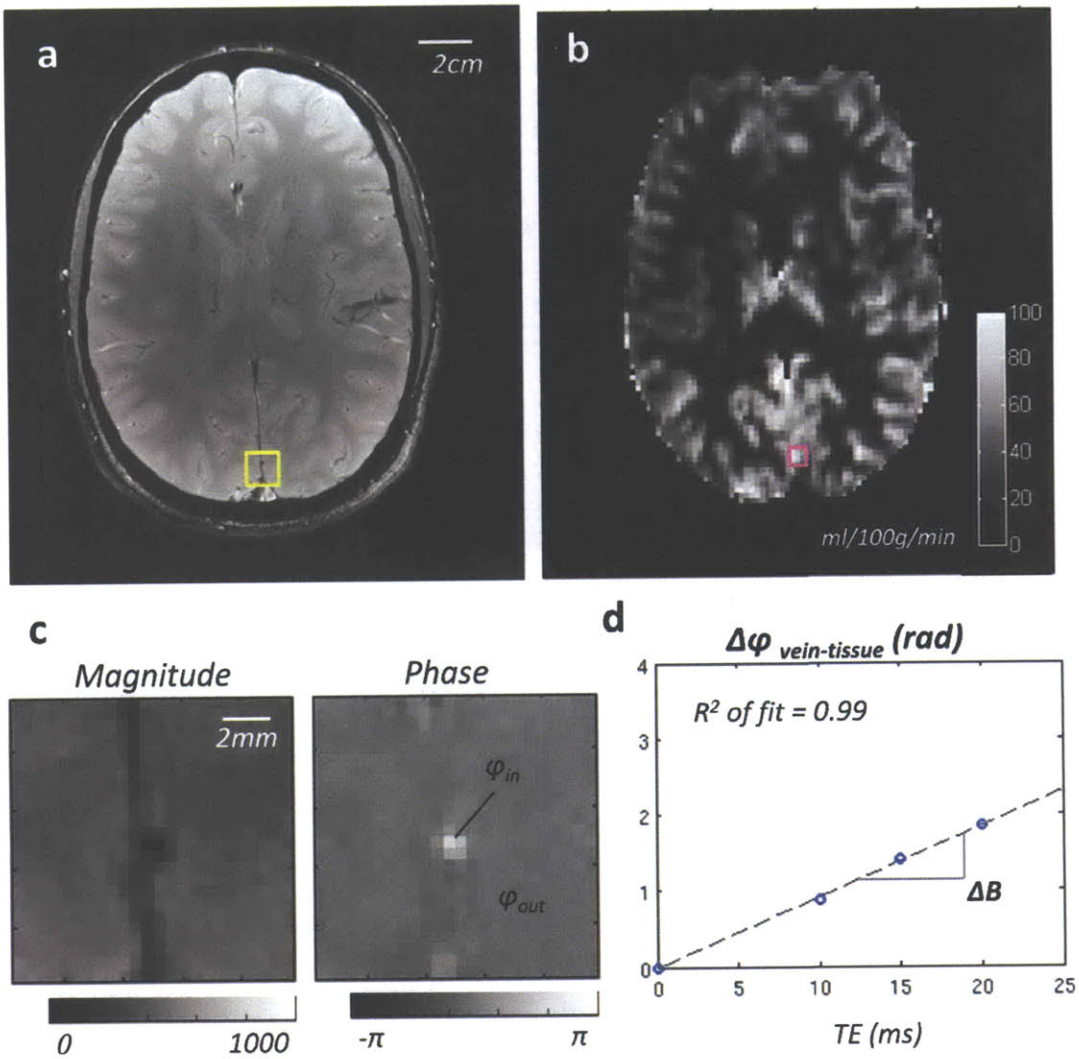

Figure 7. (**a**) Magnitude of a GRE axial slice, with region of interest (ROI) containing candidate vein highlighted in yellow box. (**b**) Corresponding CBF map from ASL acquisition. Magenta box indicates region over which perfusion values were averaged to quantify local perfusion for vessel identified in 6a. (**c**) Magnitude and phase ROI of selected vessel. Note the bright contrast of the vessel in the phase image. (**d**) Fit of measured $\Delta\varphi_{vein\text{-}tissue}$ across several echo times to quantify local ΔB.

3.4.1 Acquisition parameters for GRE and ASL at 7T

We acquired 32 axial slices with the 3D GRE sequence described in *Table 3a.* Note that we reduced both the in-plane resolution and slice thickness, and used a shorter set of TE's to

avoid phase wraps as discussed previously (*Fig 4b*). CBF maps were created using the ASL sequence described in *Table 4a*.

Table 3.

a. GRE sequence parameters at 7T

Sequence	*swi3d1r*	**Acquisition time (min)**	4:10
TR (ms)	26	**Field of view (mm)**	168 x 192
TE (ms)	6, 10, 14	**Resolution (mm)**	0.33 x 0.33 x 1.0
Flip Angle (deg)	15	**Bandwidth per pixel (Hz/pix)**	130

b. PICORE-Q2TIPS ASL sequence parameters at 7T

Sequence	*ep414A2d1*	**Acquisition time (min)**	8:42
TR (ms)	2300	**Field of view (mm)**	192 x 192
TI_1 /TI_2 (ms)	700 / 1800	**Resolution (mm)**	2.0 x 2.0 x 4.0
TE (ms)	16	**Bandwidth per pixel (Hz/pix)**	2265

3.4.2 High-pass filtering of phase images at 7T

At 7T, we first unwrapped phase images using FSL *prelude*, a fast, automated phase unwrapping algorithm based on a region merging approach [37]. Phase images were effectively high-pass filtered by subtracting a smoothed version of the phase from the original image [38]. Smoothing was done in k-space with a Gaussian low-pass filter of standard deviation $\sigma = 4$. GRE images with an ROI around a candidate vessel are illustrated in *Fig 6*.

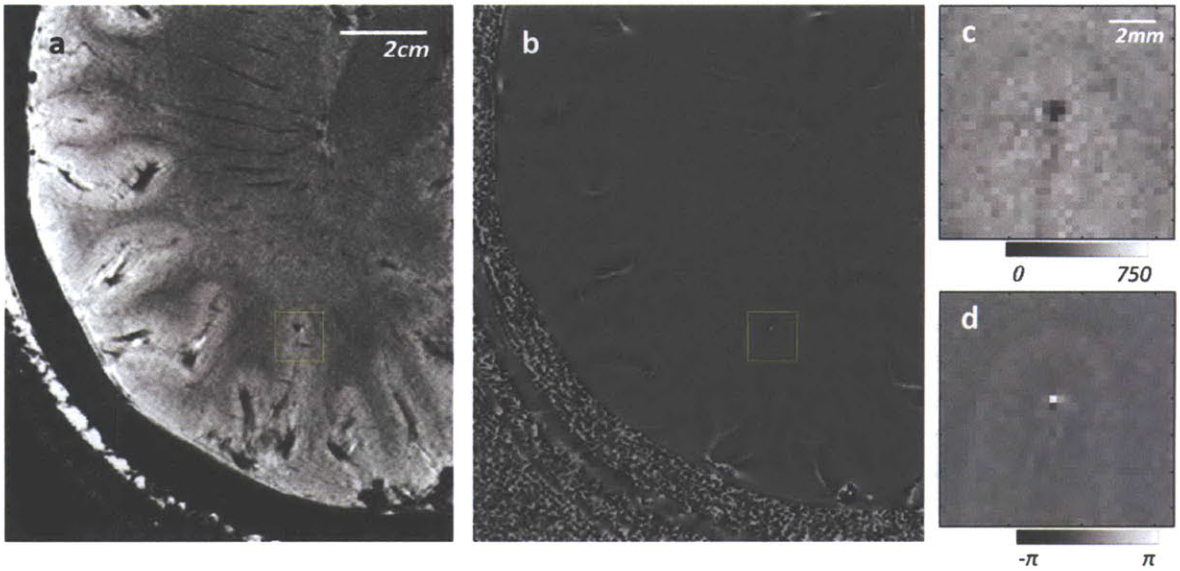

Figure 8. (**a**, **b**) Magnitude and unwrapped phase of GRE acquisition at 7T. Yellow box indicates vessel of interest. (**c, d**) Magnitude and phase ROI of candidate vessel at 7T.

Chapter 4

Results

4.1 Measurements of Y_v and $CMRO_2$ at 3T

We quantified Y_v and $CMRO_2$ in 9 healthy, young volunteers (5 male, 4 female) aged 23-32 at 3T. Data was acquired on a Siemens 3T Tim Trio 60 cm whole-body MRI. All scanning was performed under informed consent with the approval of the Institutional Review Board.

4.1.1 Study averages at 3T

For each subject, we quantified Y_v and local $CMRO_2$ for at least 5 candidate veins in the gray matter. These measurements were averaged for each subject, and study means are presented in *Table 4*. Our mean venous oxygenation (58.5%) and CBF (52.5 ml/100g/min) lie within the normal physiological range reported previously [39, 40].

Table 4. Study averages of Y_v, CBF, and $CMRO_2$ at 3T (n = 9)

Y_v (%)	CBF (ml/100g/min)	$CMRO_2$ (μmol/100g/min)
58.5 ± 2.3	52.5 ± 3.9	182 ± 15

4.1.2 Comparison of measured $CMRO_2$ to literature values

The mean $CMRO_2$ value (182 μmol/100g/min) we measure lies in the expected range from values reported in literature by PET [41-45] and the TRUST MRI method [12] as depicted in *Fig 8*. Currently, TRUST is the only other MRI-based technique to quantify $CMRO_2$. TRUST uses a tagging scheme similar to ASL for T_2 measurements in the sagittal sinus, which is the main draining vein located behind the brain [39]. These T_2 measurements are then used to quantify whole-brain Y_v through a calibration curve based on a known relationship between oxygenation and blood T_2.

Because TRUST is a whole-brain technique, its measured $CMRO_2$ values represent an average of metabolism in gray matter and white matter tissue [12]. Gray matter tissue has been shown to have higher metabolism than white matter tissue [41]. Our $CMRO_2$ measurement is slightly higher than that of TRUST, which is consistent with our focus on gray matter vessels in this study.

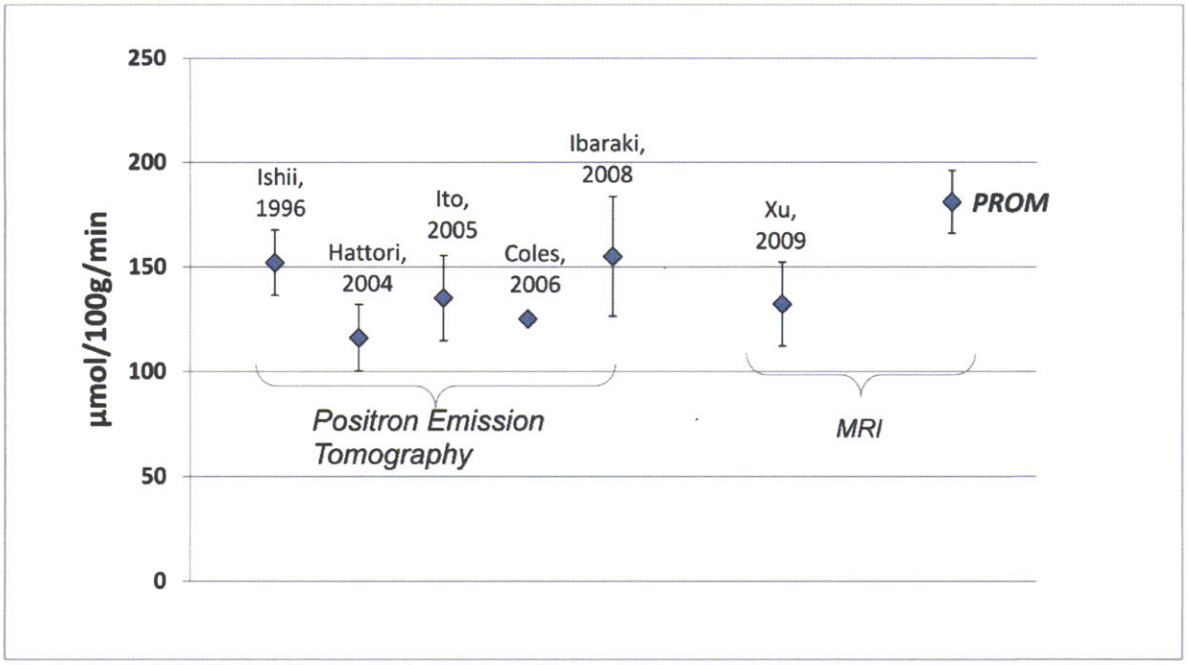

Figure 9. Comparison of measured $CMRO_2$ values to those reported by PET and MRI techniques. Our method is reported as phase-based regional oxygen metabolism (PROM).

4.2 Preliminary measurements at 7T

The improved SNR at 7T allowed us to dramatically push the resolution of our technique with a 1/5 reduction in voxel size in the GRE acquisition. We were also able to increase our coverage of the brain and quantify more vessels per subject with similar scan duration at 7T compared to 3T (*Table 5a*). Six subjects were scanned at 7T, with a mean oxygenation across the subjects of 59.7% (*Table 5b*). This matches our measured average for Y_v at 3T. We were only able to quantify $CMRO_2$ in one subject at 7T because of difficulties in EPI stability and field inhomogeneities in the inversion pulse. Our $CMRO_2$ in one subject of 162 µmol/100g/min also lies within the expected range.

Table 5.

a. Comparison of GRE acquisitions at 3T and 7T

	3T	7T
Resolution (*mm*)	0.5 x 0.5 x 2.0	0.33 x 0.33 x 1.0
Acquisition time (*min*)	5:53	4:10
Average # vessels per subject	5.8	14.0

b. Measurements of Y_v and $CMRO_2$ at 7T

Mean Y_v (n = 6):	59.7 ± 4.2 %
$CMRO_2$ in one subject:	162 *μmol/100g/min*

Chapter 5

Discussion

We have developed a new MRI method to quantify *in vivo* local Y_v and $CMRO_2$ in the brain and demonstrated the method with imaging studies on human volunteers. These physiological parameters are currently unavailable using noninvasive MRI techniques, and have the potential to provide novel information about brain function and disease. Our technique is powerful because it uses standard GRE and ASL sequences already available on most clinical scanners to make these measurements. Our measurements of Y_v and $CMRO_2$ at 3T lie within the physiological range and show promising results when compared to other techniques.

Our method is intrinsically resolution dependent and can take advantage of improved SNR at 7T for higher spatial resolution. A critical benefit of the higher resolution is mitigation of partial-volume effects, i.e. mixing of tissue types within a voxel, which can distort phase measurements that underlie our quantification of Y_v. This improved spatial resolution allows us to analyze smaller cerebral vessels expected to be more indicative of regional brain function and enables a larger number of vessels to be included in the processing. We successfully developed

an acquisition scheme and appropriate post-processing filtering to address the more difficult inhomogeneities and background susceptibility effects at high field. Here we demonstrated imaging with a 1/5 reduction in voxel size compared to 3T and dramatically increased the number of vessels analyzed for Y_v estimates, with promising physiological measurements at 7T.

One current limitation of our technique is its dependence on vessel geometry and orientation. To simplify the quantification of susceptibility, we have focused on vessel segments that can be approximated with an infinite cylinder and that are parallel to the main magnetic field. This condition naturally limits the set of vessels that can be analyzed with the current technique, and may introduce bias to our Y_v measurements depending on how well the infinite-cylinder approximation holds. In follow-up work to this thesis, we propose a detailed analysis on the effect of vessel length, tilt, and geometry on Y_v in the future to understand this potential bias.

To further address this vessel geometry limitation, we also suggest the development of quantitative susceptibility mapping (QSM) specifically for the curved vessel problem, much along the line of techniques currently being developed in the field [17–22] with applications to iron quantification in the brain. In particular, L1-weighted regularization of the inversion of field maps to susceptibility maps have been successful for mapping of regional iron deposition [38]. From magnetostatics, we know that susceptibility shifts cause perturbations in the main magnetic field and T_2* decay. Because susceptibility shifts that are not manifested in T_2* images are spatially smooth, and therefore "sparse" in an appropriate basis set, we can use L1-norm regularization to fit for a spatial susceptibility distribution [46]. This is framed as a minimization problem using a conjugate gradient optimization technique. We therefore suggest the use of

QSM to extend our analysis of Y_v to a larger set of vessels with arbitrary orientation and geometry.

Another limitation of our method is the relatively low resolution of CBF maps from which local perfusion values are quantified. ASL is intrinsically a low-resolution technique because the perfusion weighting in the ASL difference signal derives from small CBF-dependent changes between control and tag images. At 3T, our ASL acquisition uses in-plane resolution that is four times lower than the GRE sequence and has twice the slice thickness. In our analysis, we selected gray matter ROIs for average CBF corresponding to a vein identified in the GRE images. We selected this gray matter ROI to avoid partial-volume effects from white matter CBF, based on the contrast available in the perfusion map. However, it is likely that our technique still averages gray and white matter perfusion in quantifying local CBF due to its low resolution and averaging for regional CBF. Further work on characterizing these effects on our estimates is likely to be valuable.

In addition, although we calculated regional CBF using an ROI corresponding to an identified vessel, we do not know if this local ROI in fact corresponds to the tissue or territory that the vein is draining. Identifying the appropriate draining territory for a vein in the perfusion map is a more difficult task. This region of drainage likely depends on vessel size and its position within the vasculature, and determines the optimal ROI for accurate local CBF measurements. This is an interesting physiology question that we propose as valuable and high-impact future work. An understanding of vessel drainage would allow us to accurately match perfusion values in tissue to appropriate veins throughout the whole brain, and potentially extend our method to create maps of local $CMRO_2$ in the brain.

An important next step in the future development of the proposed technique is to verify the ability of our Y_v and $CMRO_2$ measurements to detect local and global physiological changes in the brain. We will assess the ability of our maps to detect localized neural activations in response to stimuli such as a visual or motor task. Global changes in Y_v and $CMRO_2$ will also be investigated using gas experiments such as hypercapnia. A key clinical collaborator at the Athinoula A. Martinos Center for Biomedical Imaging, Caterina Maneiro, M.D., recently submitted a grant proposal to the Multiple Sclerosis (MS) Society for a study in which we plan to assess physiological changes in patients with MS. Our method was proposed as an ideal candidate to investigate the chronic cerebrospinal venous insufficiency hypothesis, which suggests that venous drain blockage in the brain is critical to the pathology of MS [47]. These experiments are important to validate our Y_v and $CMRO_2$ measurements as a method for functional imaging of neural activation and disease states of the brain.

References

[1] Logothetis NK. "What we can do and what we cannot do with fMRI." *Nature* (453) 2008: 869-878.

[2] Ogawa S, Lee TM, Kay AR, Tank DW. "Brain magnetic resonance imaging with contrast dependent on blood oxygenation." *Proc Natl Acad Sci* (87) 1990: 9868-9872.

[3] Kwong KK, Belliveau JW, Chesler DA, Goldberg IE, Weisskoff RM, Poncelet BP, Kennedy DN, Hoppel BE, Cohen MS, Turner R, Cheng HM, Brady TJ, Rosen BR. "Dynamic magnetic resonance imaging of human brain activity during primary sensory stimulation." *Proc Natl Acad Sci* (89) 1992: 5675-5679.

[4] Ogawa S, Menon RS, Tank DW, Kim SG, Ellerman JM, Ugurbil K. "Functional brain mapping by blood oxygen level-dependent contrast magnetic resonance imaging." *Biophys J* (64) 1993: 803-812.

[5] van Zijl PC, Eleff SM, Ulatowski JA, Oja JM, UluĞ AM, Traystman RG, Kauppinen RA. "Quantitative assessment of blood flow, blood volume, and blood oxygenation effects in Functional magnetic resonance imaging." *Nat Med* (4) 1998: 159-167.

[6] Viswanathan A, and Freeman RD. "Neurometabolic coupling in cerebral cortex reflects synaptic more than spiking activity." *Nature Neurosci* (10) 1997, 1308-1312.

[7] Thompson JK, Peterson MR, Freeman RD. "Single-neuron activity and tissue oxygenation in the cerebral cortex." *Science* (299) 2003: 1070-1072.

[8] Leenders KL, Perani D, Lammertsma AA, Heather JD, Buckingham P, Healy MJ, Gibbs JM, Wise RJ, Hatazawa J, Herold S. "Cerebral blood flow, blood volume and oxygen utilization. Normal values and effect of age." *Brain* (113) 1990: 27-47.

[9] Sobesky J, Weber OZ, Lehnhardt FG, Hesselmann V, Neveling M, Jacobs A, Heiss WD. "Does the mismatch match the penumbra?" *Stroke* (36) 2005: 980-985.

[10] Miles KA, and Williams RE. "Warburg revisited: imaging tumour blood flow and metabolism." *Cancer Imaging* (8) 2008: 81-86.

[11] Chiarelli PA, Bulte DP, Wise R, Gallichan D, Jezzard P. "A calibration method for quantitative BOLD fMRI based on hyperoxia." *Neuroimage* (37) 2007:808–820.

[12] Xu F, Ge Y, Lu H. "Noninvasive quantification of whole-brain cerebral metabolic rate of oxygen ($CMRO_2$) by MRI. " *Magn Reson Med* (62) 2009: 141-148.

[13] Haacke EM. "In vivo measurement of blood oxygen saturation using magnetic resonance imaging: A direct validation of the blood-oxygen level-dependent concept in functional brain imaging." *Human Brain Mapping* (5) 1997: 341-346.

[14] Fernández-Seara MA, Techawiboonwong A, Detre JA, Wehrli FW. "MR susceptometry for measuring global brain oxygen extraction." *Magnetic Resonance in Medicine* (55) 2006: 967-973.

[15] Çavuşoğlu M, Pfeuffer J, Uğurbil K, Uludağ K. "Comparison of pulsed arterial spin labeling encoding schemes and absolute perfusion quantification." *Magn Reson Imaging* (27) 2009: 1039-1045.

[16] Oja JM, Gillen JS, Kauppinen RA, Kraut M, van Zijl PC. "Determination of oxygen extraction ratios by magnetic resonance imaging." *J Cereb Blood Flow Metab.* (12) 1999 :1289-1295.

[17] de Rochefort L, Brown R, Prince MR, Wang Y. "Quantitative MR susceptibility mapping using piece-wise constant regularized inversion of the magnetic field." *Magn Reson Med* (60) 2008: 1003-1009.

[18] Liu T, Spincemaille P, de Rochefort L, Kressler B, Wang Y. "Calculation of susceptibility through multiple orientation sampling (COSMOS): a method for conditioning the inverse problem from measured magnetic field map to susceptibility source image in MRI." *Magn Reson Med* (61) 2009: 196-204.

[19] Shmueli K, de Zwart JA, van Gelderen P, Li TQ, Dodd SJ, Duyn JH. "Magnetic Susceptibility Mapping of Brain Tissue In Vivo Using MRI Phase Data." *Magn Reson Med* (62) 2009: 1510–1522.

[20] Kressler B, de Rochefort L, Liu T, Spincemaille P, Jiang Q, Wang Y. "Nonlinear regularization for per voxel estimation of magnetic susceptibility distributions from MRI field maps." *IEEE Trans Med Imaging* (29) 2009: 273-281.

[21] Liu J, Liu T, de Rochefort L, Khalidov I, Prince M, Wang Y. "Quantitative susceptibility mapping by regulating the field to source inverse problem with a sparse prior derived from the Maxwell Equation: validation and application to brain." *Proc Int Soc Magn Reson Med* 2010.

[22] de Rochefort L, Brown R, Prince MR, Wang Yi. "Quantitative MR susceptibility mapping using piece-wise constant regularized inversion of the magnetic field." *Magn Reson Med* (60) 2010: 1003-1009.

[23] Schenck JF. "The role of magnetic susceptibility in magnetic resonance imaging: MRI magnetic compability of the first and second kinds." *Medical Physics* (23) 1996: 815-850.

[24] Weisskoff RM, Kiihne S. "MRI susceptometry: image-based measurement of absolute susceptibility of MR contrast agents and human blood." *Magn Reson Med* (24) 1992: 375-383.

[25] Guyton AC, and Hall JE. Textbook of Medical Physiology, 10th ed. *W. B. Saunders Company* 2000: 150.

[26] Salomir R, De Senneville BD, Moonen CTW. "A fast calculation method for magnetic field inhomogeneity due to an arbitrary distribution of bulk susceptibility." *Concepts Magn Reson B* (19B) 2003:26–34.

[27] Marques JM, Bowtell R. "Application of a Fourier-Based Method for Rapid Calculation of Field Inhomogeneity Due to Spatial Variation of Magnetic Susceptibility" *Concepts Magn Reson B* (25B) 2005: 65–78.

[28] Bernstein MA, King KF, Zhou XJ. Handbook of MRI Pulse Sequences. *Elsevier Academic Press* 2004: 579-606.

[29] Haase A, Frahm J, Matthaei D, Haenicke W, Merboldt KD. "Flash imaging. Rapid NMR imaging using local flip angle pulses." *J Magn Reson* (67) 217-225: 1986.

[30] Williams DS, Detre JA, Leigh JS, Koretsky AP. "Magnetic resonance imaging of perfusion using spin inversion of arterial water." *Proc Natl Acad Sci USA* (89) 1992: 212-216.

[31] Edelman RR, Siewert B, Darby DG, Thangaraj V, Nobre AC, Mesulam MM, Warach S. "Quantitative mapping of cerebral blood-flow and functional localization with echo-planar MR imaging and signal targeting with alternating radio-frequency." *Radiology* (192) 1994: 513-520.

[32] Wong EC, Buxton RB, Frank LR. "Implementation of quantitative perfusion imaging techniques for functional brain mapping using pulsed arterial spin labeling." *Nucl Magn Reson Biomed* (10) 1997: 237-249.

[33] Wong EC, Buxton RB, Frank LR. "Quantitative imaging of perfusion using a single subtraction (QUIPSS AND QUIPSS II)." *Magn Reson Med* (39) 1998: 702-708.

[34] Luh WM, Wong EC, Bandettini PA, Hyde JS. "QUIPSS II with thin-slice TI1 periodic saturation: a method for improving accuracy of quantitative perfusion imaging using pulsed arterial spin labeling." *Magn Reson Med* (41) 1999:1246–1254.

[35] Wang J, Alsop DC, Listerud J, Gonzalez-At JB, Schnall MD, Detre JA. "Comparison of quantitative perfusion imaging using arterial spin labeling at 1.5 and 4.0 Tesla." *Magn Reson Med* (48) 2002: 242-254.

[36] Wang Y, Yu Y, Li D, Bae KT, Brown JJ, Lin W, Haacke EM. "Artery and vein separation using susceptibility-dependent phase in contrast-enhanced MRA." *J Magn Reson Imaging* (12) 2000: 661-670.

[37] Jenkinson M. "Fast, automated, *N*-dimensional phase-unwrapping algorithm." *Magn Reson Med* (49) 2003: 193-197.

[38] Rauscher A, Barth M, Herrmann KH, Witoszynskyj S, Deistung A, Reichenbach JR. "Improved elimination of phase effects from background field inhomogeneities for susceptibility weighted imaging at high magnetic field strengths." *Magn Reson Imaging* (26) 2008: 1145-1151.

[39] Lu H and Ge Y. "Quantitative evaluation of oxygenation in venous vessels using T2-relaxation-under-spin-tagging MRI." *Magn Reson Med* (60) 2008: 357-363.

[40] Peterson ET, Mouridsen K, Golay X. "The QUASAR reproducibility study, Part II: Results from a multi-center arterial spin labeling test-retest study." *Neuroimage* (49) 2010: 104-113.

[41] Ishii K, Sasaki M, Kitagaki H, Sakamoto S, Yamaji S, Maeda K. "Regional difference in cerebral blood flow and oxygen metabolism in human cortex." *J Nucl Med* (37) 1996: 1086-1088.

[42] Hattori N, Bergsneider M, Wu HM, Glenn TC, Vespa PM, Hovda DA, Phelps ME, Huang SC. "Accuracy of a method using short inhalation of (15)O-O(2) for measuring cerebral oxygen extraction fraction with PET in healthy humans." *J Nucl Med* (45) 2004: 765-770.

[43] Ito H, Kano I, Fukuda H. "Human cerebral circulation: positron emission tomography studies." *Ann Nucl Med 2005* (19) 2005 65-74.

[44] Coles JP, Fryer TD, Bradley PG, Nortje J, Smielewski P, Rice K, Clark JC, Pickard JD, Menon DK. "Intersubject variability and reproducibility of 15O PET studies." *J Cereb Blood Flow Metab* (26) 48-57.

[45] Ibaraki M, Miura S, Shimosegawa E, Sugawara S, Mizuta T, Ishikawa A, Amano M. "Quantification of cerebral blood flow and oxygen metabolism with 3-dimensional PET and 15O: validation by comparison with 2-dimensional PET." *J Nucl Med* (49) 2008: 50-59.

[46] Lustig M, Donoho D, Pauly JM. "Sparse MRI: The application of compressed sensing for rapid MR imaging." *Magn Reson Med* (58) 2007: 1182-1195.

[47] Zamboni P, Galeotti R, Malagoni AM, Tacconi G, Dall'Ara S, Bartolomei I, F Salva. "Chronic cerebrospinal venous insufficiency in patients with multiple sclerosis." *J Neurol Neurosurg Psychiatry* (80) 2009: 392-399.